RSC Advances

PAPER

View Article Online
View Journal | View Issue



Cite this: *RSC Adv.*, 2017, **7**, 4547

# Room-temperature pulsed CVD-grown $SiO_2$ protective layer on $TiO_2$ particles for photocatalytic activity suppression

Jing Guo,[ab] Shaojun Yuan,[a] Yangyang Yu,[a] J. Ruud van Ommen,[b] Hao Van Bui[b] and Bin Liang*[a]

Received 9th December 2016
Accepted 3rd January 2017

DOI: 10.1039/c6ra27976g

www.rsc.org/advances

This work presents a novel chemical vapor deposition (CVD) approach that enables the deposition of ultrathin and conformal $SiO_2$ layers on $TiO_2$ anatase nanoparticles at room temperature using $SiCl_4$ and air containing water without the use of a catalyst. The morphology of the CVD-grown $SiO_2$ layers was found to be strongly dependent on the initial surface states of the $TiO_2$ nanopowders, which could be altered by applying a simple heat pretreatment. The deposition on untreated $TiO_2$ resulted in granular films, whereas on preheated $TiO_2$ highly uniform and conformal $SiO_2$ layers were obtained. By varying the $SiCl_4$ precursor dosing time and the number of CVD cycles, the thickness of the $SiO_2$ could be controlled at the nanometer level, which allowed us to investigate the influence of film thickness on the photocatalytic suppression ability. We found that a conformal $SiO_2$ layer with a thickness of 3 nm could sufficiently suppress the photocatalytic activity of anatase $TiO_2$ nanoparticles, which was demonstrated by the photodegradation of Rhodamine B. Our approach offers a simple, fast, feasible and low-temperature deposition method which can be directly applied to $SiO_2$ coating on nanoparticles in pigments and other fields, particularly heat-sensitive materials, and further developed for large-scale production.

## 1 Introduction

Nanoparticulate titanium dioxide ($TiO_2$) is the most commonly-used white pigment in the paint, plastic, and paper industries due to its high brightness, high refractive index and photostability.[1,2] However, the high photocatalytic activity of $TiO_2$ facilitates the oxidation and decomposition of organic compounds, for instance, in the paint layer, which consequently changes the color and severely decreases the lifetime of the products.[3] Therefore, in these practical applications, $TiO_2$ nanoparticles (NPs) are commonly coated with a thin insulating layer to suppress their photocatalytic activity. On the one hand, this coating layer is required to sufficiently block the transport of electrons and holes, which are generated in the $TiO_2$ particles under UV-light irradiation, to the surface that initiates the photocatalytic reactions with organic compounds. On the other hand, the coating layer must not affect the bulk optical properties of the $TiO_2$ pigment. Owing to their large band gap, high thermal and optical stabilities, and chemical inertness, ceramic oxides, such as $Al_2O_3$, $SiO_2$, $CeO_2$ and $ZrO_2$, have been popularly used as coating materials on $TiO_2$ for photocatalytic suppression.[4–14]

Various strategies have been developed to deposit thin metal oxide films on $TiO_2$ pigment particles. Among them, wet chemistry methods, such as sol–gel and precipitation, have been extensively used due to their simplicity, inexpensiveness and versatility in producing various materials with tunable properties.[4–6,8,15,16] For instance, Ren *et al.* employed sol–gel method in the presence of 3-hydroxytyramine hydrochloride, poly(-diallyldimethylammonium chloride), poly(sodium 4-styreneslfonate), tetraethyl orthosilicate (TEOS) and solvents to fabricate $TiO_2/SiO_2$ core/shell particles.[6] Upon exposure to UV radiation, a rattle-type structure with tunable catalytic/UV-shielding properties was obtained. The $TiO_2/SiO_2$ core/shell structure for UV radiation shielding can also be obtained by the conventional Stöber method using TEOS and solvents such as ethanol, $NH_4OH$ and acetone.[4,5] Binary $Al_2O_3/SiO_2$ coating layers have been deposited on $TiO_2$ nanoparticles using sol–gel and precipitation mothods for enhanced brightness and whiteness of $TiO_2$.[8,16] Moreover, wet chemistry methods enable the deposition of various ceramic and transition metal oxide materials such as $ZrO_2$, $CeO_2$, NiO and CoO on $TiO_2$ particles.[15] Nevertheless, these methods have several shortcomings in controlling the coating thickness and conformality due to their high sensitivity to experimental parameters, such as precursor concentration, type and pH of the solvents, deposition time and temperature. In

[a]*Multi-phase Mass Transfer & Reaction Engineering Lab, College of Chemical Engineering, Sichuan University, Chengdu 610065, China. E-mail: liangbin@scu.edu.cn; Fax: +86-28-85460556; Tel: +86-28-85460556*

[b]*Department of Chemical Engineering, Delft University of Technology, Delft, The Netherlands*

addition, these methods are time consuming and normally require post-treatment processes, for instance, high temperature treatment, washing, drying, and separation to eliminate impurities that arise from the residual solvent and reaction byproducts.[5,6] These disadvantages hinder the applicability of wet chemistry in the syntheses of metal oxide layers on $TiO_2$ in practical applications. It is therefore of importance to search for a facile, low-cost, and efficient approach for deposition of metal oxide layers on the $TiO_2$ particles.

Gas-phase deposition techniques such as chemical vapor deposition (CVD) and atomic layer deposition (ALD) have been attractive alternatives in recent years. ALD is based on the sequential exposures of the support/substrate to precursors in the gas phase. This enables self-limiting surface reactions and provides the ability to control the amount of depositing materials down to atomic level with high uniformity and conformality in many applications.[17,18] ALD has also been applied for coating $Al_2O_3$ and $SiO_2$ films on $TiO_2$ nanoparticles for catalytic suppression.[12–14] With ALD, ultrathin and conformal $SiO_2$ and $Al_2O_3$ layers with a thickness of several nanometers can be achieved, showing excellent stability and high efficiency in suppressing the catalytic properties of $TiO_2$ nanoparticles.[12,13] Molecular layer deposition (MLD), the organic counterpart of ALD, has also been applied for depositing aluminum alkoxide (*i.e.*, alucone) using trimethylaluminum and ethylene glycol as precursors. This alucone layer can reduce the undesired color change of the white pigment $TiO_2$, which was observed for the $TiO_2$ coated with $SiO_2$ and $Al_2O_3$ layers by ALD.[14]

CVD of $SiO_2$ thin films has been extensively investigated over the past decades.[10,11,19–25] TEOS, silane ($SiH_4$), dichlorosilane ($SiCl_2H_2$) and silicon tetrachloride ($SiCl_4$) are among the most popularly used precursors in conjunction with $H_2O$ or $O_2$ as oxidizing agent. This has been used to deposit thin $SiO_2$ layers on $TiO_2$ micro- and nanoparticles.[10,23,26,27] Powell *et al.* demonstrated CVD of $SiO_2$ films at a temperature in the range of 1300–1500 °C employing the $SiCl_4/O_2$ chemistry, and found that the film surface was smoother at a higher temperature and in the absence of water.[11,26,27] Using the same $SiCl_4/O_2$ chemistry, Simpson *et al.* reported that ultrathin and continuous $SiO_2$ layers with a thickness of 1–2 nm could be obtained at 1000 °C.[10] By replacing $O_2$ with $H_2O$ as the oxidizing agent, Tsapatsis and Gavalas demonstrated that the deposition temperature of $SiO_2$ CVD could be significantly reduced to approximately 600 °C.[23] It can be concluded that CVD of $SiO_2$ generally requires an elevated temperature. Remarkably, Klaus and George found that the use of $NH_3$ as catalyst for the $SiCl_4/H_2O$ CVD process could enable the deposition of $SiO_2$ at room temperature.[24] To the best of our knowledge, this is so far the only room-temperature $SiO_2$ CVD process using $SiCl_4$ precursor reported in literature.

Accordingly, the main aim of this work is to develop a novel approach that enables the room-temperature CVD (RTCVD) of $SiO_2$. We demonstrate that ultrathin and conformal $SiO_2$ layers on $TiO_2$ nanoparticles can be deposited at room temperature using $SiCl_4$ and air containing water without the use of catalysts. As $SiCl_4$ can react robustly with $H_2O$, the use of air containing water is to decelerate the reaction kinetics and achieve a better control of deposition rate. Therefore, the thickness of coating layers can be controlled at nanometer scale by varying the $SiCl_4$ dosing time and the number of CVD cycles. We found that the morphology of the coating layers, *i.e.*, granular or continuous films, is strongly influenced by initial surface states of the $TiO_2$ nanopowders, which can be altered by applying a simple heat treatment at a relatively low temperature (*i.e.*, 170 °C). Photocatalytic tests are performed on the as-synthesized $SiO_2/TiO_2$ nanoparticles to evaluate the catalytic suppression ability of the room-temperature CVD-grown $SiO_2$, and to study the influence of coating thickness on the suppression ability. The results obtained from our work demonstrate a simple, fast and feasible method for coating $SiO_2$ on $TiO_2$ pigment, which is applicable for other powders and can be further developed for large-scale production.

# 2 Experimental

## 2.1. Materials

Anatase $TiO_2$ powders with diameter in the range of 200–300 nm and specific surface area of about 10.7 $m^2\ g^{-1}$ (determined by BET technique) were provided by Taihai $TiO_2$ pigment Co. (Panzhihua, China). Rhodamine B (RhB) and silicon tetrachloride ($SiCl_4$) were purchased from Sigma-Aldrich (St. Louis, MO, USA). The $TiO_2$ powders and the chemicals were used as received without any additional treatment or purification.

## 2.2. Preparation of $SiO_2$-coated $TiO_2$ nanoparticles

The coating apparatus and deposition steps are schematically shown in Fig. 1. $TiO_2$ powders, without or with heat pretreatment at 170 °C for 1 h (*i.e.*, performed *ex situ* in an oven prior to the CVD), were supported on a porous distributor plate, and were immobilized inside a glass reactor with volume of 1 L (Fig. 1a). The thickness of the $TiO_2$ layer on the distributor plate is about 2 mm. At this thickness and with a long dosing time (*i.e.*, up to 60 min), the diffusion limitation of the gas molecules to the bottom of the layer can be eliminated.[28] Before introducing $SiCl_4$, the reactor was slowly evacuated to a pressure of 70 mbar using a mechanical pump. This was to create a pressure difference between the chamber and the $SiCl_4$ vapor precursor (*ca.* 260 mbar at room temperature). $SiCl_4$ was then fed into the reactor (V1 opened, V2 and V3 closed) with dosing times varying from 3 to 60 min to react with the hydroxyl groups (–OH) on the surface of $TiO_2$ nanoparticles (Fig. 1b–d). Hereafter, the excess precursor, if any, and the reaction byproducts (*i.e.*, HCl) were removed (V1 and V2 closed, V3 opened). Air containing $H_2O$ vapor (*i.e.*, 44% RH) was then introduced into the chamber and maintained at atmospheric pressure to react with the Si–Cl terminated surface, forming an $SiO_2$ layer and creating an –OH terminated surface (Fig. 1e), which is necessary for the chemisorption of $SiCl_4$ in the next cycle. The use of air containing $H_2O$ vapor instead of pure $H_2O$ is due to the fact that $SiCl_4$ can react robustly with $H_2O$, which could lead to the uncontrollable deposition.

## 2.3. Material characterization

The thickness of the $SiO_2$ layers on the $TiO_2$ particles was measured by transmission electron microscopy (TEM) using

 

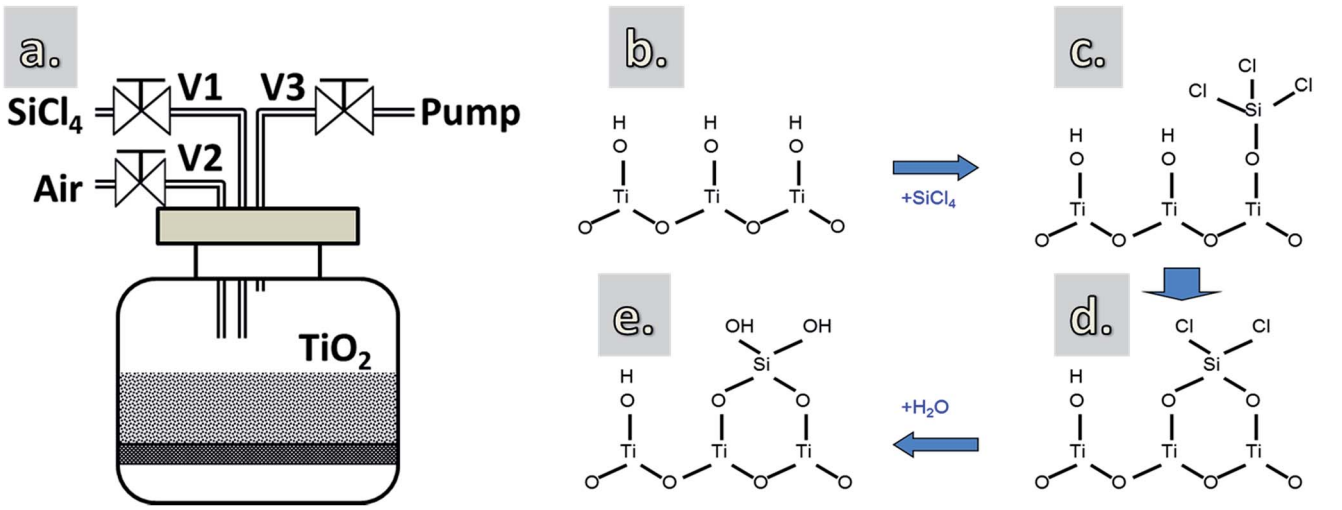


Fig. 1 A schematic drawing of the reactor (a) and the proposed growth mechanism of $SiO_2$ using $SiCl_4$ and $H_2O$ vapor (b–e).

a JEOL JEM1400 operating at a voltage of 120 kV and a current density of 50 pA $cm^{-2}$. The composition of the $SiO_2$ layers was characterized by X-ray photoelectron spectroscopy (XPS) (XSAM800, Kratos, UK) with monochromatized Al Kα radiation at constant dwell time of 100 ms and pass energy of 55 eV. The peaks positions were calibrated according to the C 1s peak at 284.8 eV. The infrared spectra were acquired using FTIR spectroscopy (Spectrum II L1600300 spectrometer, PerkinElmer) in transmission mode.

### 2.4. Photocatalytic activity determination

The photocatalytic activity of the $SiO_2$-coated $TiO_2$ powders was evaluated by the photodegradation of RhB solution. For each test, 150 mg powders were added to 30 mL RhB solution (concentration of 9 mg $L^{-1}$) and continuously stirred in the dark for 30 min to obtain a uniform suspension. Thereafter, the suspension was exposed to UV radiation generated by a mercury lamp with a power of 300 W or 500 W for different exposure times. The set-up allowed to carry out up to 10 samples simultaneously, which ensured that all samples were irradiated under the same conditions, such as light intensity, exposure time, and temperature. The suspension was then centrifuged to separate the powders from the solution. Finally, the solution was analyzed by UV-visible spectrophotometry to determine the residual concentration of the RhB in solution, which was used to evaluate the catalytic activity suppression of the $SiO_2$ layers.

## 3 Results and discussion

### 3.1. Reaction mechanism

The chemical reactions in CVD of $SiO_2$ using $SiCl_4$ and $H_2O$ are generally described as:[24]

$$SiCl_4 + 2H_2O \rightarrow SiO_2 + 4HCl \quad (1)$$

However, it has been reported that the actual growth of $SiO_2$ CVD consists of a number of reactions, which can be divided into homogeneous and heterogeneous reactions.[22,23] Homogeneous reactions occur between $SiCl_4$ and $H_2O$ molecules in the gas phase, forming oligomers or particles. These reactions have slow kinetics.[22,23,29] The heterogeneous reactions take place directly on the surface *via* substitution reactions of surface groups (*i.e.*, –Cl and –OH groups). In this case, the reactions are described as:[22,23]

$$|\text{–OH(s)} + SiCl_4(g) \rightarrow |\text{–O–Si–Cl(s)} + HCl(g) \quad (2)$$

$$|\text{–O–Si–Cl(s)} + H_2O(g) \rightarrow |\text{–O–Si–OH(s)} + HCl(g) \quad (3)$$

where |–OH(s) and |–Si–Cl(s) represent the surface hydroxyl and chlorosilicon groups, respectively. In addition to these reactions, condensation reactions simultaneously take place between two –OH groups or –OH and Si–Cl groups on the surface to form siloxane bonds (Si–O–Si), described as:[22,23]

$$|\text{–O–Si–OH(s)} + |\text{–O–Si–Si–OH(s)} \rightarrow \text{Si–O–Si(s)} + H_2O(g) \quad (4)$$

$$|\text{–O–Si–OH(s)} + |\text{–O–Si–Si–Cl(s)} \rightarrow \text{Si–O–Si(s)} + HCl(g) \quad (5)$$

Therefore, CVD of $SiO_2$ using $SiCl_4$ and $H_2O$ might consist of gas-phase reactions, substitution reactions of surface functional groups and condensation reactions.

### 3.2. Morphology and composition of the coating layers

Tsapatsis *et al.* postulated that the surface morphology of the coating layer is influenced by the reactant species, *i.e.*, $H_2O$ molecules (vapor and physisorbed $H_2O$) and –OH groups (chemisorbed $H_2O$). Accordingly, the reactions between $SiCl_4$ and $H_2O$ molecules may lead to the formation of a granular surface.[22,23] However, this has not been experimentally demonstrated. Here, we observed that the deposition of $SiO_2$ on $TiO_2$ particles without pretreatment resulted in granular and porous surfaces (Fig. 2a). This is attributed to the presence of a thick hydration shell with abundant physisorbed $H_2O$ and –OH groups on the particle surface,[30] as detected by FTIR spectra (Fig. 2c). The peak at 3400 $cm^{-1}$ is attributed to the stretching vibration of –OH groups ($\nu_{O-H}$) on the surface of $TiO_2$ particles, whereas the peak at

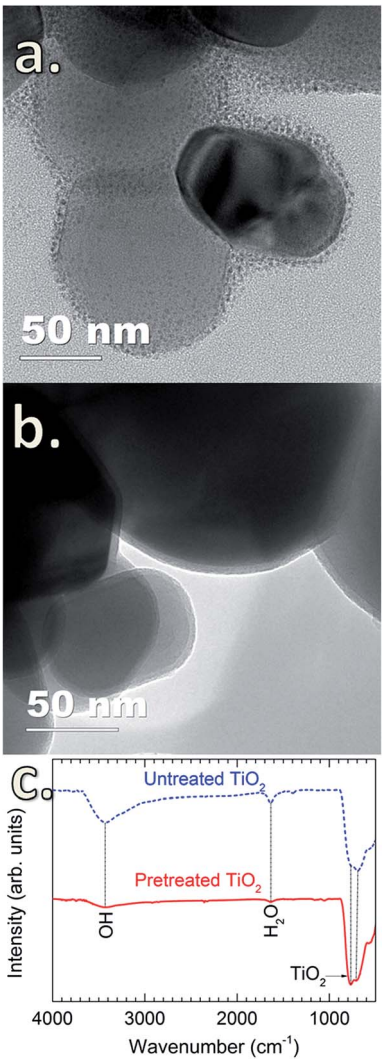


Fig. 2 TEM images of $SiO_2$-coated anatase $TiO_2$ particles (a) without heat pretreatment and (b) with heat pretreatment at 170 °C for 1 h, and (c) FTIR spectra of the $SiO_2$-coated $TiO_2$ particles without and with heat pretreatment. CVD reaction conditions: $SiCl_4$ dosing time of 60 min and air exposure time of 60 min. The average thickness of the $SiO_2$ coating layer is 3.4 ± 0.1 nm.

1625 $cm^{-1}$ corresponds to the bending vibration of physisorbed $H_2O$ molecules ($\delta_{H_2O}$).[31,32] In the fingerprint region (*i.e.*, wavenumber below 1000 $cm^{-1}$), the peaks located in the wavenumber range of 500–700 $cm^{-1}$ are ascribed to the bending vibration of Ti–O–Ti ($\delta_{Ti-O-Ti}$) of the $TiO_2$ particles.[31] Upon the heat pretreatment of $TiO_2$ particles at 170 °C for 1 h, the intensity of the characteristic peaks of $\nu_{O-H}$ and $\delta_{H_2O}$ significantly decreases (Fig. 2c), indicating that a large amount of the physisorbed $H_2O$ molecules and –OH groups has desorbed from the $TiO_2$ surface.[33–37] Therefore, for the untreated $TiO_2$ particles, the physisorbed $H_2O$ can react with $SiCl_4$ to form $SiO_2$ following reaction (1), and in accordance with the previous assumption by Tsapatsis *et al.*, a granular film is formed.[22] In comparison with the previous findings that the reaction between $SiCl_4$ and $H_2O$ either required high temperatures[22] or the presence of catalysts to enable the deposition at room temperature,[24] our work has demonstrated the deposition of $SiO_2$ at room temperature without the use of catalyst. This is probably due to the higher pressure range in the reactor, as well as the catalytic $TiO_2$ surface. Klaus and George also observed that increasing $H_2O$ partial pressure resulted in the enhanced deposition of $SiO_2$ in $SiCl_4$/$H_2O$ CVD.[24] Nevertheless, this requires further studies to verify, which is out of the scope of this work. On the pretreated $TiO_2$ particles, highly uniform, continuous and dense $SiO_2$ films are formed (Fig. 2b), which is substantially different from the porous and granular $SiO_2$ films on the untreated $TiO_2$ particles. This is ascribed to the different reaction mechanism. CVD of $SiO_2$ on the pretreated $TiO_2$ particles proceeds following the reactions (2)–(5) (*i.e.*, *via* surface reactions with |–OH and |–Cl groups), thus resulting in the formation of continuous and dense layers.

Fig. 3 shows the O 1s and Ti 2p core-level XPS spectra of uncoated and $SiO_2$-coated $TiO_2$ powders. For the uncoated $TiO_2$, the O 1s spectrum is fitted to two peaks with binding energies (BE) at 529.5 and 530.8 eV (Fig. 3a) corresponding to the O–Ti and O–H chemical states, respectively.[38] This is consistent with the results obtained from FTIR shown in Fig. 2c. The O 1s spectrum of the $SiO_2$-coated $TiO_2$ shows a noticeable difference with an intense peak at 532.69 eV, representing the Si–O chemical state in $SiO_2$.[39] The fitted spectrum also reveals the presence of additional components located at 534.5 eV (Si–$O_x$) and 531.64 eV (Si–O–Ti).[39] No significant change was observed for the Ti 2p spectra of uncoated and $SiO_2$-coated $TiO_2$ particles. In addition, no considerable amount of Cl contamination was detected by XPS, suggesting the complete consumption of –Cl by the chemical reactions with $H_2O$.

The presence of $SiO_2$ is additionally confirmed by the FTIR spectra obtained for $TiO_2$ powders coated with $SiO_2$ layers with different $SiCl_4$ dosing times (Fig. 4). The characteristics of $SiO_2$ are represented by the two sharp peaks at 1227 and 1080 $cm^{-1}$.[5] The results show that the absorption increases drastically with the increase of $SiCl_4$ dosing time from 3 to 30 min, which is indicative of the increase of the coating thickness consistent with the results obtained from TEM (Fig. 5). The images indicate that highly uniform and conformal $SiO_2$ layers with a thickness as thin as 1 nm can be achieved, which is commonly difficult to obtain by conventional CVD. With increasing dosing time from 7 to 30 min, the coating thickness rises rapidly from 1.4 to 3.0 nm, and gradually reaches saturation with the further increase of dosing time. This saturation may be caused by the complete consumption of the –OH functional groups and adsorbed $H_2O$ on the surface by $SiCl_4$, which consequently terminates the chemical reactions. A small increase in thickness with increasing dosing time from 30 to 60 min is attributed to the contribution of the residual $H_2O$ vapor inside the chamber and the condensation reactions described above (*i.e.*, reactions (4) and (5)).

### 3.3. Catalytic suppression of $SiO_2$ coating layers

Fig. 6a shows the photocatalytic activity toward the degradation of RhB of the uncoated $TiO_2$ and the $TiO_2$ coated with $SiO_2$ layers obtained for different $SiCl_4$ dosing times. Prior to the UV irradiation, the solution was constantly stirred in the dark (light-off stage) for 30 min to obtain uniform particle dispersion. The

 

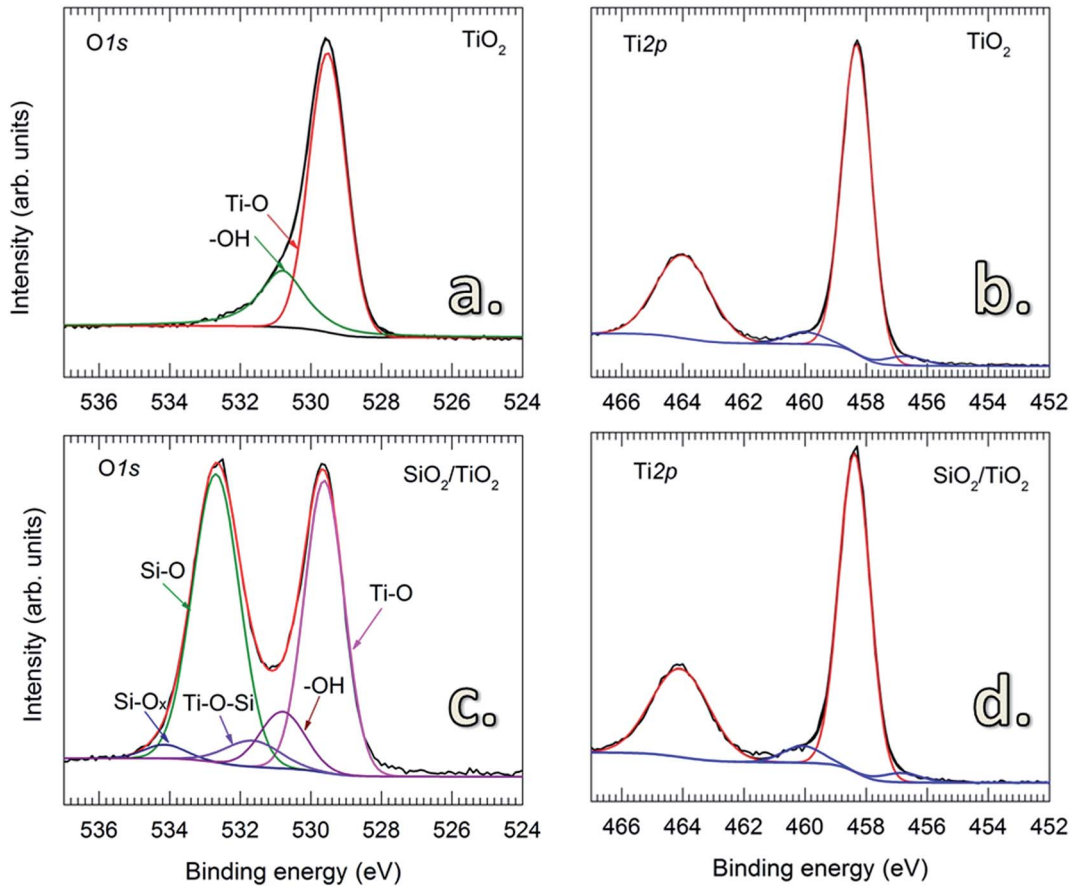


Fig. 3 XPS spectra of O 1s and Ti 2p of uncoated (a and b) and $SiO_2$-coated $TiO_2$ (c and d) powders. CVD was performed on pretreated $TiO_2$ particles with $SiCl_4$ dosing time of 15 min and air exposure time of 60 min.

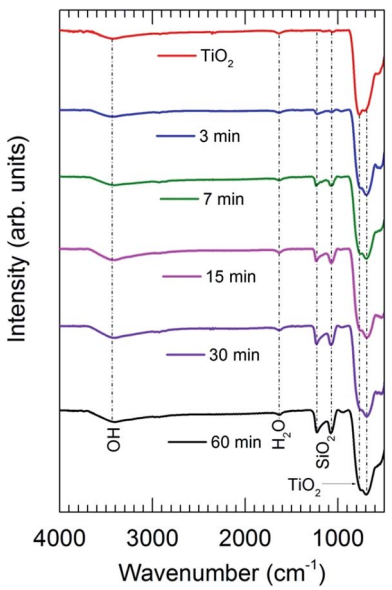


Fig. 4 FTIR spectra of the uncoated $TiO_2$ and $SiO_2$-coated $TiO_2$ with different $SiCl_4$ dosing times. CVD was performed on pretreated $TiO_2$ particles with an air exposure time of 60 min.

samples were collected after certain time-intervals to determine the concentration of the remaining RhB. In the absence of $TiO_2$ powders, the results show that during this stage, the concentration of RhB remained unchanged. However, a small drop of RhB concentration was observed for the solutions with $TiO_2$ powders (both uncoated and coated with $SiO_2$). This drop is caused by the adsorption of a fraction of RhB molecules on the surface of the particles. Thereafter, upon the exposure to UV radiation (light-on stage), the concentration of RhB decayed rapidly for the uncoated powders, indicating the high photocatalytic activity of $TiO_2$. Similar effects were observed for the $TiO_2$ coated with $SiO_2$ deposited with short $SiCl_4$ dosing times (up to 15 min). This could be due to the insufficient thickness of the coating and/or the devoid pin-hole free films. As shown in Fig. 5a and b, the thickness of the $SiO_2$ layers for short dosing times is 2 nm or less (*i.e.*, 1.4 and 2.0 nm for 7 and 15 min of dosing time, respectively). $SiO_2$ films with a thickness of 3 nm and thicker obtained for longer $SiCl_4$ dosing times showed significant improvement in the suppression of $TiO_2$ photocatalytic activity. The small decrease in RhB concentration observed for these two powders (*i.e.*, with $SiO_2$ layers obtained for 30 and 60 min $SiCl_4$ exposures) is nearly identical to the decrease observed for RhB without powders, which is attributed to the self-degradation of RhB under the UV irradiation. This is better indicated by the reaction kinetic

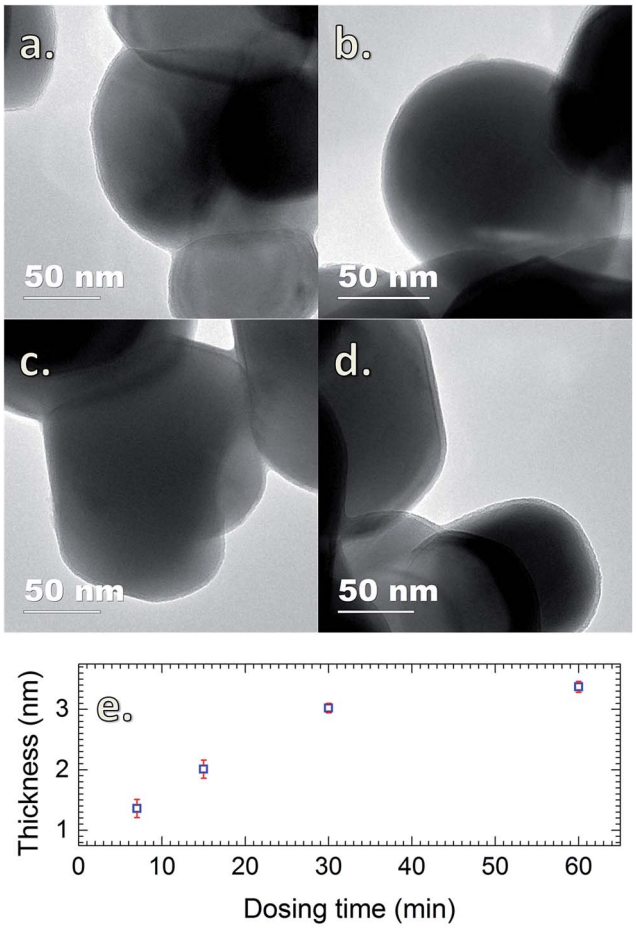


Fig. 5 TEM images of $SiO_2$-coated $TiO_2$ particles with different $SiCl_4$ dosing times: 7 min (a), 15 min (b), 30 min (c) and 60 min (d). (e) shows the increasing trend of the coating thickness with dosing time. CVD was performed on pretreated $TiO_2$ particles.

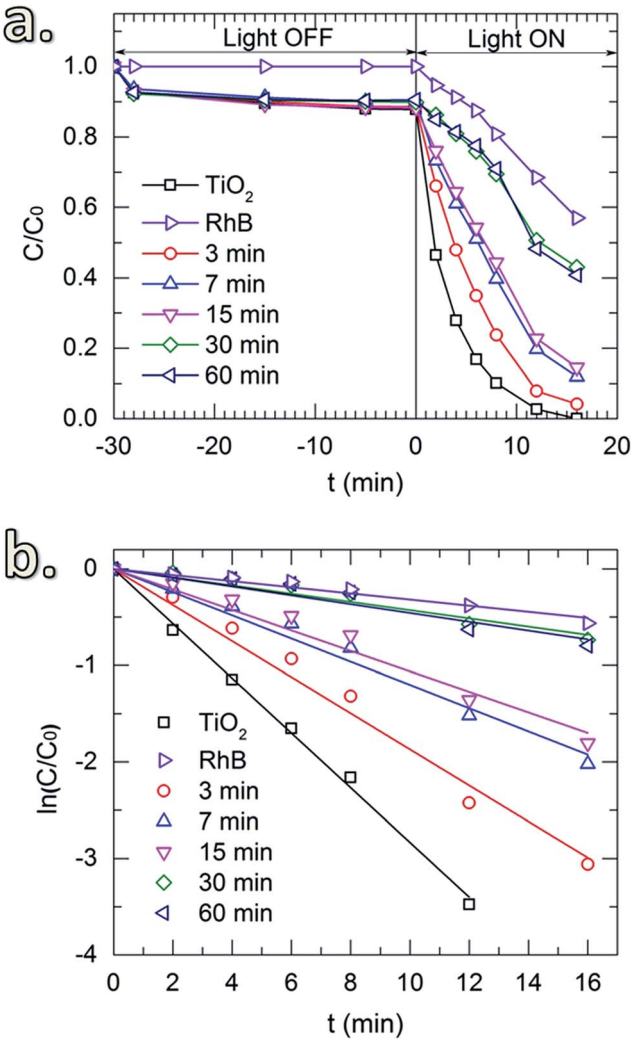


Fig. 6 The photocatalytic degradation of RhB under 500 W UV light using $SiO_2$-coated $TiO_2$ powders with different $SiCl_4$ dosing times (a) and the corresponding reaction kinetic plots (b). The $k_{app}$ values are extracted from the slopes of the linear fitting of the measured data.

plots shown in Fig. 6b obtained from the kinetic equation described as:[40]

$$\ln(C_0/C) = k_{app}t, \text{ or } C = C_0 \exp(-k_{app}t) \quad (6)$$

where $k_{app}$ is the apparent first-order kinetic constant, which represents the reaction rate. From eqn (6), $k_{app}$ value for each reaction can be extracted from the slope of the linear fitting (Table 1). The results show that the $k_{app}$ values obtained for the powders coated with $SiO_2$ with long $SiCl_4$ dosing times are only slightly higher than that of the RhB self-degradation (0.043 and 0.046 compared to 0.032 of RhB), suggesting good catalytic activity suppression by these coatings. In other words, a film thickness of above 3 nm ensures sufficient photocatalytic suppression. The enhancement of the catalytic suppression for the longer dosing time may be ascribed partially to the reconstruction of the layers during the exposure. As discussed above, the small increase in $SiO_2$ thickness with increasing dosing time might be attributed to the condensation reactions of the precursor molecules (*i.e.*, reactions (4) and (5) in Section 3.1), which create siloxane bonds (Si–O–Si), resulting in fewer pinholes and denser films. This consequently increases the suppression ability of the coating layers. The results from TEM imaging show that the surface morphology of the coating layer was unaffected by the photocatalytic reactions (not shown), indicating the stability of the coating layer.

Table 1 Apparent first-order rate constant, $k_{app}$, of $TiO_2$ powders coated with $SiO_2$ with different $SiCl_4$ dosing times

| Dosing time/min | $k_{app}$/min$^{-1}$ | $R^2$ of fitting |
|---|---|---|
| 0 (uncoated $TiO_2$) | 0.283 ± 0.004 | 0.99 |
| 3 | 0.187 ± 0.006 | 0.99 |
| 7 | 0.120 ± 0.005 | 0.99 |
| 15 | 0.106 ± 0.005 | 0.98 |
| 30 | 0.043 ± 0.003 | 0.97 |
| 60 | 0.046 ± 0.004 | 0.95 |
| RhB (without powders) | 0.032 ± 0.002 | 0.98 |

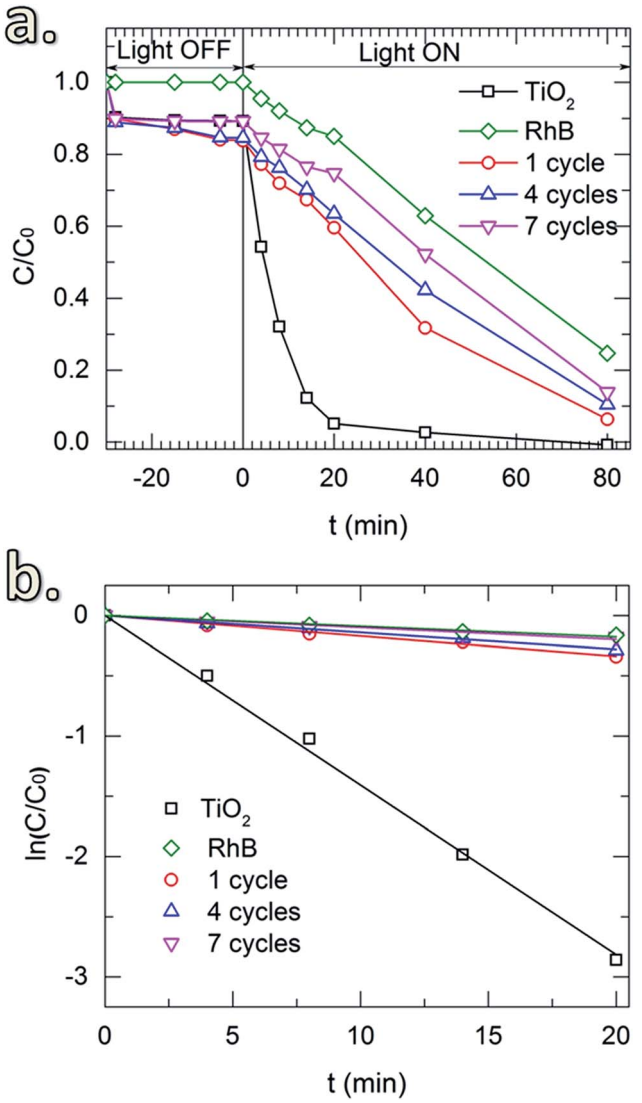


Fig. 7 Photocatalytic degradation of RhB under 300 W UV light using $SiO_2$-coated $TiO_2$ powders with different number of $SiO_2$ CVD cycles (1, 4 and 7). CVD reaction conditions: $SiCl_4$ dosing time of 30 min and air exposure time of 60 min.

Fig. 7 shows the RhB degradation of the $SiO_2$-coated $TiO_2$ with different numbers of coating cycles. In this case, an $SiCl_4$ dosing time of 30 min was applied for all of the depositions. Samples for 1, 4 and 7 cycles were tested. In addition, the UV irradiation power was reduced to 300 W to enable the study of the degradation up to 80 min. The same drop of RhB concentration caused by the surface adsorption was observed in the light-off stage (Fig. 7a). In the light-on stage, the reaction kinetic plots (Fig. 7b) show negligible effect of thickness on the photocatalytic degradation, demonstrating the sufficient suppression of the $SiO_2$ layers deposited with a small number of CVD cycles. In comparison with the materials and coating methods that have been used to mitigate the photocatalytic activity of $TiO_2$ pigmentary materials (Table 2), our approach showed several advantages in providing a fast, simple and efficient process. Especially, for the first time in literature a room-temperature gas-phase deposition technique for pigmentary coating applications is introduced.

## 4 Conclusions

We have demonstrated the room-temperature pulsed-CVD of $SiO_2$ thin films on $TiO_2$ nanoparticles using $SiCl_4$ as the Si precursor and air containing water vapor as the oxidizing agent without the use of catalysts. The formation of $SiO_2$ was confirmed by XPS and FTIR spectroscopy. The deposition on the $TiO_2$ powders without preheating resulted in a granular surface, whereas on pretreated $TiO_2$ (at 170 °C for 1 h) highly uniform, conformal and continuous $SiO_2$ films were obtained. The thickness of the $SiO_2$ layer increased with $SiCl_4$ dosing time and reached saturation most likely upon the consumption of the surface hydroxyl groups and water vapor. This enabled the control of coating thickness at nanometer level precision, and consequently, the study of the influence of film thickness on photocatalytic suppression ability of $SiO_2$ films. Accordingly, we found that a minimum thickness of about 3 nm is needed to sufficiently suppress the photocatalytic properties of $TiO_2$

Table 2 Thin film coating methods and materials for suppressing photocatalytic activity of $TiO_2$ pigmentary materials

| $TiO_2$ material | Coating method | Coating material | Coating thickness (nm) | Deposition temperature (°C) | Photocatalytic reaction | Ref. |
|---|---|---|---|---|---|---|
| P25 | ALD | $Al_2O_3$ | 6 | 177 | Methylene blue | 41 |
| Anatase | ALD | $SiO_2$ | 2 | 500 for $SiO_2$ | IPA to acetone | 12 |
| | | $SiO_2/Al_2O_3$ | 1/1 | 177 for $Al_2O_3$ | | |
| | | $SiO_2/Al_2O_3/SiO_2/Al_2O_3$ | 0.5/0.5/0.5/0.5 | | | |
| P25 | ALD | $Al_2O_3$ | 3.8 | 150 | RhB | 42 |
| Anatase | ALD | $SiO_2$ | 6 | 175 | Methylene blue | 13 |
| P25 | | | 9 | | | |
| Anatase | MLD | Alucone | 7–10 | 100–160 | Methylene blue | 14 |
| Rutile | CVD | $SiO_2$ | 1–2 | 900–1000 | Methylene blue | 10 |
| Rutile | Wet-chemistry | $ZrO_2$ | 5 | 40 | RhB | 15 |
| | | $CeO_2$ | 1–2 | 60 | | |
| Rutile | Wet-chemistry | $CeO_2$ | 1–2 | 60 | RhB | 43 |
| ST-21 | Wet-chemistry | $SiO_2$ | 4 | 40 | Methylene blue | 4 |
| P25 | Wet-chemistry | Porous $SiO_2$ | 20 | Room temperature | RhB | 6 |
| Anatase | Pulsed-CVD | $SiO_2$ | 3 | Room temperature | RhB | This work |

toward the degradation of RhB. A further increase in film thickness resulted in only insignificant improvement in the suppression performance. Our work has demonstrated a simple, fast and feasible method for depositing $SiO_2$ on $TiO_2$ pigment at room temperature, which is applicable also for other powders, especially for heat-sensitive materials, and can be further developed for large-scale production.

## Acknowledgements

The authors would like to acknowledge the financial support of key project of National Natural Science Foundation of China (No. 21236004), and China Scholarship Council.

## References

1 H. Shi, R. Magaye, V. Castranova and J. Zhao, *Part. Fibre Toxicol.*, 2013, **10**, 15–47.
2 C. L. Bianchi, C. Pirola, F. Galli, G. Cerrato, S. Morandi and V. Capucci, *Chem. Eng. J.*, 2015, **261**, 76–82.
3 X. Feng, S. Zhang and X. Lou, *Colloids Surf., B*, 2013, **107**, 220–226.
4 H. Lee, S. Koo and J. Yoo, *J. Ceram. Process. Res.*, 2012, **13**, S300–S303.
5 O. K. Park and Y. S. Kang, *Colloids Surf., A*, 2005, **257**, 261–265.
6 Y. Ren, M. Chen, Y. Zhang and L. Wu, *Langmuir*, 2010, **26**, 11391–11396.
7 Y. Liu, C. Ge, M. Ren, H. Yin, A. Wang, D. Zhang, C. Liu, J. Chen, H. Feng and H. Yao, *Appl. Surf. Sci.*, 2008, **254**, 2809–2819.
8 Y. Zhang, H. Yin, A. Wang, M. Ren, Z. Gu, Y. Liu, Y. Shen, L. Yu and T. Jiang, *Appl. Surf. Sci.*, 2010, **257**, 1351–1360.
9 H.-X. Wu, T.-J. Wang and Y. Jin, *Ind. Eng. Chem. Res.*, 2006, **45**, 5274–5278.
10 D. J. Simpson, A. Thilagam, G. P. Cavallaro, K. Kaplun and A. R. Gerson, *Phys. Chem. Chem. Phys.*, 2011, **13**, 21132–21138.
11 Q. H. Powell, T. T. Kodas and B. M. Anderson, *Chem. Vap. Deposition*, 1996, **2**, 179–181.
12 D. M. King, X. Liang, B. B. Burton, M. K. Akhtar and A. W. Weimer, *Nanotechnology*, 2008, **19**, 255604–255611.
13 X. Liang, K. S. Barrett, Y.-B. Jiang and A. W. Weimer, *ACS Appl. Mater. Interfaces*, 2010, **2**, 2248–2253.
14 X. Liang and A. W. Weimer, *J. Nanopart. Res.*, 2010, **12**, 135–142.
15 B.-X. Wei, L. Zhao, T.-J. Wang, H. Gao, H.-X. Wu and Y. Jin, *Adv. Powder Technol.*, 2013, **24**, 708–713.
16 B.-X. Wei, L. Zhao, T.-J. Wang and Y. Jin, *Ind. Eng. Chem. Res.*, 2011, **50**, 13799–13804.
17 S. M. George, *Chem. Rev.*, 2010, **110**, 111–131.
18 H. Van Bui, F. Grillo and J. R. van Ommen, *Chem. Commun.*, 2017, **53**, 45–71.
19 F. S. Becker, D. Pawlik, H. Anzinger and A. Spitzer, *J. Vac. Sci. Technol., B*, 1987, **5**, 1555–1563.
20 A. Adams and C. Capio, *J. Electrochem. Soc.*, 1979, **126**, 1042–1046.
21 K. Watanabe, T. Tanigaki and S. Wakayama, *J. Electrochem. Soc.*, 1981, **128**, 2630–2635.
22 M. Tsapatsis, S. Kim, S. W. Nam and G. R. Gavalas, *Ind. Eng. Chem. Res.*, 1991, **30**, 2152–2159.
23 M. Tsapatsis and G. R. Gavalas, *AIChE J.*, 1992, **38**, 847–856.
24 J. W. Klaus and S. M. George, *J. Electrochem. Soc.*, 2000, **147**, 2658–2664.
25 S. Chaudhary, A. R. Head, R. Sánchez-de-Armas, H. Tissot, G. Olivieri, F. Bournel, L. Montelius, L. Ye, F. Rochet, J.-J. Gallet, B. Brena and J. Schnadt, *J. Phys. Chem. C*, 2015, **119**, 19149–19161.
26 Q. H. Powell, G. P. Fotou, T. T. Kodas and B. M. Anderson, *Chem. Mater.*, 1997, **9**, 685–693.
27 Q. H. Powell, G. P. Fotou, T. T. Kodas, B. M. Anderson and Y. Guo, *J. Mater. Res.*, 1997, **12**, 552–559.
28 D. Longrie, D. Deduytsche and C. Detavernier, *J. Vac. Sci. Technol., A*, 2014, **32**, 010802.
29 M. L. Hair and W. Hertl, *J. Phys. Chem. C*, 1969, **73**, 2372–2378.
30 V. N. Koparde and P. T. Cummings, *J. Phys. Chem. C*, 2007, **111**, 6920–6926.
31 S. Musić, M. Gotić, M. Ivanda, S. Popović, A. Turković, R. Trojko, A. Sekulić and K. Furić, *Mater. Sci. Eng., B*, 1997, **47**, 33–40.
32 S. Sivakumar, P. K. Pillai, P. Mukundan and K. G. K. Warrier, *Mater. Lett.*, 2002, **57**, 330–335.
33 S. Benkoula, O. Sublemontier, M. Patanen, C. Nicolas, F. Sirotti, A. Naitabdi, F. Gaie-Levrel, E. Antonsson, D. Aureau, F.-X. Ouf, S.-I. Wada, A. Etcheberry, K. Ueda and C. Miron, *Sci. Rep.*, 2015, **5**, 15088.
34 M. A. Henderson, *Langmuir*, 1996, **12**, 5093–5098.
35 L. Walle, A. Borg, P. Uvdal and A. Sandell, *Phys. Rev. B: Condens. Matter Mater. Phys.*, 2009, **80**, 235436.
36 S. Wendt, R. Schaub, J. Matthiesen, E. K. Vestergaard, E. Wahlström, M. D. Rasmussen, P. Thostrup, L. M. Molina, E. Lægsgaard, I. Stensgaard, B. Hammer and F. Besenbacher, *Surf. Sci.*, 2005, **598**, 226–245.
37 U. Aschauer, Y. He, H. Cheng, S.-C. Li, U. Diebold and A. Selloni, *J. Phys. Chem. C*, 2009, **114**, 1278–1284.
38 B. Erdem, R. A. Hunsicker, G. W. Simmons, E. D. Sudol, V. L. Dimonie and M. S. El-Aasser, *Langmuir*, 2001, **17**, 2664–2669.
39 G. Kovács, Z. Pap, C. Coteț, V. Coşoveanu, L. Baia and V. Danciu, *Materials*, 2015, **8**, 1059–1073.
40 S. Wang, F. Teng and Y. Zhao, *RSC Adv.*, 2015, **5**, 76588–76598.
41 L. F. Hakim, D. M. King, Y. Zhou, C. J. Gump, S. M. George and A. W. Weimer, *Adv. Funct. Mater.*, 2007, **17**, 3175–3181.
42 E. Jang, K. Sridharan, Y. M. Park and T. J. Park, *Chem.–Eur. J.*, 2016, **22**, 12022–12026.
43 H. Gao, B. Qiao, T.-J. Wang, D. Wang and Y. Jin, *Ind. Eng. Chem. Res.*, 2014, **53**, 189–197.

 